THE JOURNAL OF BIOLOGICAL CHEMISTRY VOL. 288, NO. 37, pp. 26357–26371, September 13, 2013
Published in the U.S.A.

Myocilin Mediates Myelination in the Peripheral Nervous System through ErbB2/3 Signaling*

Received for publication, December 18, 2012, and in revised form, July 26, 2013 Published, JBC Papers in Press, July 29, 2013, DOI 10.1074/jbc.M112.446138

Heung Sun Kwon[‡], Thomas V. Johnson[‡1], Myung Kuk Joe[‡], Mones Abu-Asab[§], Jun Zhang[§2], Chi Chao Chan[§], and Stanislav I. Tomarev[‡3]

From the [‡]Section of Retinal Ganglion Cell Biology, Laboratory of Retinal Cell and Molecular Biology, and [§]Histology Core, NEI, National Institutes of Health, Bethesda, Maryland 20892

Background: Myocilin, a secreted glaucoma-associated protein, is detected in the sciatic nerve, but its function there is not clear.
Results: *Myocilin* null mutation leads to defects in the myelination of sciatic nerve acting through the ErbB2/ErbB3 receptor.
Conclusion: Myocilin is a novel player in sciatic nerve myelination.
Significance: This is the first demonstration of myocilin involvement in myelination.

The glaucoma-associated gene, *myocilin*, is expressed in ocular and non-ocular tissues including the peripheral nervous system, but its functions in these tissues remain poorly understood. We demonstrate that in sciatic nerve, myocilin is expressed in Schwann cells with high concentrations at the nodes of Ranvier. There, myocilin interacts with gliomedin, neurofascin, and NrCAM, which are essential for node formation and function. Treatment of isolated dorsal root ganglion cultures with myocilin stimulates clustering of the nodal proteins neurofascin and sodium channel $Na_v1.2$. Sciatic nerves of myocilin null mice express reduced levels of several myelin-associated and basal membrane proteins compared with those of wild-type littermates. They also demonstrate reduced myelin sheath thickness and partial disorganization of the nodes. Myocilin signaling through ErbB2/3 receptors may contribute to these observed effects. Myocilin binds to ErbB2/ErbB3, activates these receptors, and affects the downstream PI3K-AKT signaling pathway. These data implicate a role for myocilin in the development and/or maintenance of myelination and nodes of Ranvier in sciatic nerve.

Myocilin is a secreted glycoprotein that belongs to the family of olfactomedin domain-containing proteins (1). The *MYOCILIN* (*MYOC*) gene is heavily expressed in ocular drainage structures, such as the trabecular meshwork, which is responsible for a maintaining proper balance of intraocular pressure. It is well established that mutations in the *MYOC* gene can lead to glaucoma, a major cause of blindness. *MYOC* mutations are found in >10% of juvenile open-angle glaucoma and in 3–4% of patients with adult onset primary open-angle glaucoma (2–6). The most severe mutations in *MYOC* lead to intraocular pressure elevation. Available data suggest that wild-type myocilin is not required for the physiological regulation of intraocular pressure (7–9). In particular, *Myoc* knock-out mice do not develop glaucoma and appeared to be grossly normal (8). However, more careful analyses of *Myoc* null mice showed that these mice exhibit a moderate reduction in the amount of dystrophin-associated syntrophin and reduced levels of phospo-Akt in skeletal muscle compared with wild-type littermates (10). Patients with glaucoma who carry *MYOC* mutations are not known to develop abnormal non-ocular phenotypes even though the *MYOC* gene is expressed in several non-ocular tissues (4, 6, 11, 12).

The sciatic nerve is one of the known sites of extraocular myocilin expression (13). Another olfactomedin domain-containing protein, gliomedin, is expressed by myelinating Schwann cells and is essential for molecular assembly at the nodes of Ranvier in sciatic nerve and for clustering of nodal components including voltage-gated Na^+ channels at heminodes during myelination (14–17). Gliomedin interacts with several immunoglobulin family cell adhesion molecules including NrCAM and two isoforms of neurofascin, NF155 and NF186, in an olfactomedin domain-dependent fashion (14, 15). Although clustering is critical for saltatory conduction of action potentials along myelinated axons, adult gliomedin null mice do not show any obvious neurological abnormalities and exhibit normal nerve conduction.

The aim of the present study was to characterize the role of myocilin in sciatic nerve. We demonstrate that myocilin is concentrated at the nodes of Ranvier, where it interacts with several nodal proteins. Myocilin induces clustering of the $Na_V1.2$ sodium channel and NF186 in dorsal root ganglion (DRG)[4] axons in the absence of glial cells. In sciatic nerve *in vivo*, myocilin co-localizes with and is able to physically bind the epidermal growth factor receptors ErbB2/ErbB3, resulting in phosphorylation (activation) of the receptors. Finally, the sciatic nerves of *Myoc* null mice show changes in the organization of axon bundles and partial disorganization of the nodes. These

* This work was supported by the Intramural Research Program of the NEI, National Institutes of Health.
[1] Present address: School of Medicine, Johns Hopkins University, Baltimore, MD 21205.
[2] Present address: NINDS, National Institutes of Health, Bethesda, MD 20892.
[3] To whom correspondence should be addressed: Bldg. 6, Rm. 212, 6 Center Dr., SRGCB, LRCMB, NEI, National Institutes of Health, Bethesda, MD 20892. Tel.: 301-496-8524; Fax: 301-480-2610; E-mail: tomarevs@nei.nih.gov.

[4] The abbreviations used are: DRG, dorsal root ganglion; AP, alkaline phosphatase; CM, conditioned medium; RTK, phosphor-receptor tyrosine kinase; MBP, myelin basic protein; Nrg1, neuregulin 1; PNS, peripheral nervous system.

data suggest that myocilin signaling through ErbB receptors may play a role in PNS myelination.

EXPERIMENTAL PROCEDURES

Animals—Mice were maintained in accordance with guidelines set forth by the National Eye Institute Committee on the Use and Care of Animals. *Myoc* null mice (B6/129 mixed genetic background) and transgenic mice expressing elevated levels of myocilin (C57BL/6J genetic background) have been described previously (8, 18).

DNA Constructs and Antibodies—Human FLAG- and alkaline phosphatase (AP)-tagged myocilin, myocilin-ΔC, and myocilin-ΔN constructs have been described (19). *ErbB1*, *ErbB2*, and *ErbB3* cDNAs were obtained from Addgene (Cambridge, MA). His-tagged gliomedin ectodomain construct and polyclonal gliomedin antibody were obtained from Dr. Manuel Koch (17). Antibodies were obtained from following sources: FLAG and S100 (Sigma); P0, β-dystroglycan, and HSC70 (Santa Cruz Biotechnology, CA); myelin basic protein (MBP), NrCAM, and gliomedin (Abcam); α-dystroglycan, neurofilament H, laminin β1, laminin γ1, and integrin β1 (Millipore); Krox20 (Covance); neurofascin (kindly provided by Dr. Elior Peles). Horseradish peroxidase-conjugated secondary antibodies were from GE Healthcare. Goat anti-mouse, -rabbit, and -goat labeled with Alexa488 or 594 were from Invitrogen. Myocilin antibodies were described (20).

Reverse Transcriptase-Polymerase Chain Reaction (RT-PCR)—Total RNA was extracted from postnatal day 20 (P20) sciatic nerve tissues using the RNeasy mini kit (Qiagen, CA). Ten nanograms of RNA were used for each RT-PCR reaction. RT-PCR was performed using SuperScript® III One-Step RT-PCR System with the Platinum®Taq kit according to the manufacturer's instruction (Invitrogen). Primers for the amplification of a laminin *a2* fragment were 5′-GCCAGGACATCGGGACTAT-3′ and 5′-CCAGGAGGACGCCATTCTTA-3′, for laminin *β1* were 5′-CGAGGGAGGCTGAGAAACTAA-3′ and 5′-TTCCTCCTGCTGCTCCTTGA-3, and for laminin γ1 were 5′-GCAGGTGACAAAGCCGTAGA-3′ and 5′ATCGGCTCGAGCTAGGAGTT-3′. Primers for the amplification of *GAPDH* were 5′- CCCATCACCATCTTCCAGGAGCG-3′ and 5′-CGGGAAGCTCACTGGCATGGCCT-*3*′.

Cell and Tissue Cultures—Dissociated mouse DRG cultures were grown in Neurobasal medium (Invitrogen) supplemented with B27 (Invitrogen) as described (14, 21). Briefly, DRGs of P5 mice were trypsinized, seeded on poly-D-lysine/laminin two-well cultures slides (BD Bioscience) or poly-D-lysine-coated 13-mm slides (Sigma), and grown in BN medium containing Basal medium-Eagle, ITS supplement, 0.2% bovine serum albumin (BSA), 4 mg/ml D-glucose (Sigma), glutamax (Invitrogen), 50 ng/ml NGF (Almone Labs), and antibiotics. Schwann cells were isolated as described (22). In brief, sciatic nerves of P5 mice were digested in 0.1% collagenase, 0.25% trypsin, triturated with a 1-ml pipette 10 times and then with a fire-polished pasture pipette 7 times in 10% FBS. Dissociated cells from 10 sciatic nerves were resuspended in 5 ml of DMEM with 10% FBS and plated into a 6-well plate. On the second day in culture, cells were treated with cytosine arabinoside (10^{-5} M) for 24 h to reduce fibroblast contamination. On day 4 in culture, cells were treated with glial growth factor (10 μg/ml) and forskolin (5 μM) to expand the Schwann cell population. On day 7 in culture, cells were trypsinized, washed, and plated onto polylysine-coated cover glasses in 2-well chamber slides. Three days after plating, the medium was removed, and cells were washed 2–3 times with PBS. Cells were fixed with fresh 3.7% formaldehyde for 10 min at room temperature and permeabilized with 0.1% Triton X-100 in PBS for 5 min. After blocking with 5% BSA in PBS at room temperature for 1 h, cells were incubated with anti-myocilin polyclonal (1:500 dilution) and anti-P0 monoclonal antibody (1:500 dilution) at room temperature for 1 h. Cells were washed with PBS-Tween 20 and then incubated with Alexa-488 or 594 conjugated secondary antibodies for 30 min. An Axioplan 2 fluorescent microscope and Zeiss700 confocal microscope (Carl Zeiss MicroImaging, Inc.) were used to detect fluorescence. The images were processed with Adobe Photoshop Elements 2.0 (Adobe Inc.).

Western Blot Analysis—Sciatic nerves were dissected and homogenized using a Dounce homogenizer in radioimmune precipitation assay buffer (50 mM Tris-HCl, pH 7.4, 150 mM NaCl, 1 mM EDTA, 1% Nonidet P-40, and 0.25% sodium deoxycholate) containing a mixture of protease inhibitors (Roche Applied Science) at 4 °C. Homogenates were centrifuged for 20 min at 21,000 × *g* at 4 °C. To analyze laminin levels in sciatic nerve of P22 and adult mice, a membrane protein extraction kit (Thermo Scientific) was used. Briefly, sciatic nerves were first washed with a cell wash solution and then homogenized in a permeabilization buffer at 4 °C. Homogenate was centrifuged at 16,000 × *g* for 15 min at 4 °C. The supernatant containing cytosolic proteins was removed, and the pellet was solubilized in 8 M urea-containing solubilization buffer by up and down pipetting with subsequent incubation for 30 min at 4 °C. This extract was centrifuged for 15 min at 16,000 × *g* at 4 °C, and the supernatant was used for subsequent analysis. Equal amounts of protein from each supernatant (measured with the BCA Protein Assay; Bio-Rad) were size-fractionated by SDS-PAGE, transferred to PVDF membranes, and immunoblotted. For quantification, the chemiluminescent signals were captured using an 8-megapixel scientific-grade CCD camera (Flurochem M. Santa Clara, CA), and the signal intensities were quantified and analyzed using AlphaView software (Proteinsimple, Santa Clara, CA). All Western blot experiments were performed at least three times using independent animals or pairs of littermates.

Binding Assays—AP-tagged fusion protein expression constructs were transfected into HEK293 cells to generate conditioned medium (CM)-containing AP-fusion proteins. The culture medium was changed to the fresh serum-free medium at 24 h after the transfection, and CM was harvested 24–48 h later, filtered through a 0.22-μm filter, and stored at −80 °C until use. Absolute concentration and integrity of AP-tagged myocilin was determined by Western blotting using samples with known amounts of purified myocilin. NIH3T3 cells were transfected with ErbB2, ErbB3, or vector plasmids and incubated with AP-myocilin containing CM for 90 min at room temperature 48 h after transfection. Cells were washed 5 times and fixed by treatment with 60% acetone, 3% formaldehyde, and 20 mM HEPES, pH 7.5, for 30 s, and surface binding was visualized using the AP substrate 5-bromo-4-chloro-3-indolyl

phosphate following the manufacturer's instructions (Genhunter Corp.). The images of stained cells were obtained with a dissection microscope (Zeiss, STEMI SV-11). For quantitative analysis of the activity of cell-bound AP, 1-Step™ PNPP (Pierce) was added to the fixed cells, and the absorbance at 405 nm in the supernatant was measured at 405 nm using a microplate reader (Bio-Rad, Model-680).

Coimmunoprecipitation—Sciatic nerve lysates were cleared by centrifugation at 16,000 × *g* for 15 min and were immunoprecipitated with antibodies against myocilin, ErbBs, gliomedin, or NrCAM at 4 °C overnight and then with protein-A agarose (Roche Applied Science) at room temperature for 1 h. Bound proteins were eluted from the beads by boiling in SDS-PAGE sample buffer and analyzed by Western blotting using the indicated antibodies. HEK293 cells were transiently transfected with myocilin-FLAG, gliomedin-His, or NF186-Fc using Lipofectamine 2000 (Invitrogen) and seeded in 6-well culture dishes. Cells were washed with PBS and lysed in lysis buffer 48 h after transfection. Cleared lysates were subjected to immunoprecipitation with anti-FLAG and anti-His antibodies (Sigma) and Protein-G magnetic beads (Dynal, Invitrogen). Immunoprecipitates were analyzed by Western blotting using indicated antibodies.

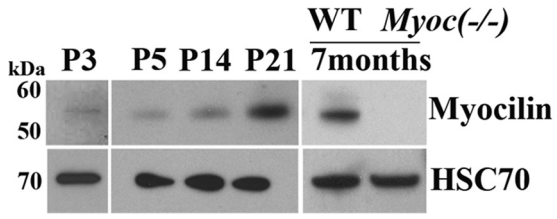

FIGURE 1. **Myocilin expression in mouse sciatic nerve.** Western blot analysis of myocilin expression in P3-P21 and 7-month-old mouse sciatic nerves is shown. Sciatic nerves from 7-month-old *Myoc* knock-out mice (*Myoc*$^{-/-}$) were used as a control for myocilin antibody specificity (1:2000 dilution). Staining of the same blot with antibodies against HSC70 (1:5000 dilution) was used for normalization of loading.

Tissue Preparation for Immunofluorescence—Sciatic nerves, spinal cords, and brains were embedded in optimal cutting temperature compound and frozen in acetone cooled with dry ice. Mice were anesthetized using a lethal dose of ketamine/xylazine (1:10) injected intraperitoneally. Anesthetized animals were perfused with a fixative containing 4% paraformaldehyde in 0.1 M phosphate buffer, pH 7.4, and the dissected tissues were fixed for 30 min in the same solution, cryoprotected by infiltration in 20% sucrose overnight, and embedded in optimal cutting temperature compound. Cryostat sections (5–10 μm thick) were thaw-mounted on Super-Frost Plus glass slides (Fisher) and stored at −20 °C. Tissue sections were fixed in 4% PBS-buffered paraformaldehyde and permeabilized with 0.3% Triton X-100 and 3% goat serum in PBS. Samples were incubated with primary antibodies diluted in PBS containing 3% goat serum at 4 °C overnight. After washing with PBS for 3 times, samples were incubated with Alexa Fluor 488 goat anti-rabbit or Alexa Fluor 594 goat anti-mouse secondary antibody for 1 h at room temperature. Samples were mounted using Vectashield mounting medium (Vector), and images were taken using a Zeiss LSM700 confocal microscope with a 40× objective lens. Images were scanned using ZEN software (Zeiss) and quantified using NIH image J software.

Electron Microscopy—Mice were anesthetized using a lethal dose of ketamine/xylazine (1:10) injected intraperitoneally. Anesthetized animals were perfused with a fixative containing 4% paraformaldehyde, 2.5% glutaraldehyde, 0.13 M NaH_4PO_4, and 0.11 M NaOH, pH 7.4. Perfused tissues were fixed in PBS-buffered 2.5% glutaraldehyde and 0.5% osmium tetroxide, dehydrated, and embedded into Spurr's epoxy resin. Ultrathin sections (90 nm) were made, double-stained with uranyl acetate and lead citrate, and viewed in a JEOL JEM 1010 (Tokyo, Japan)

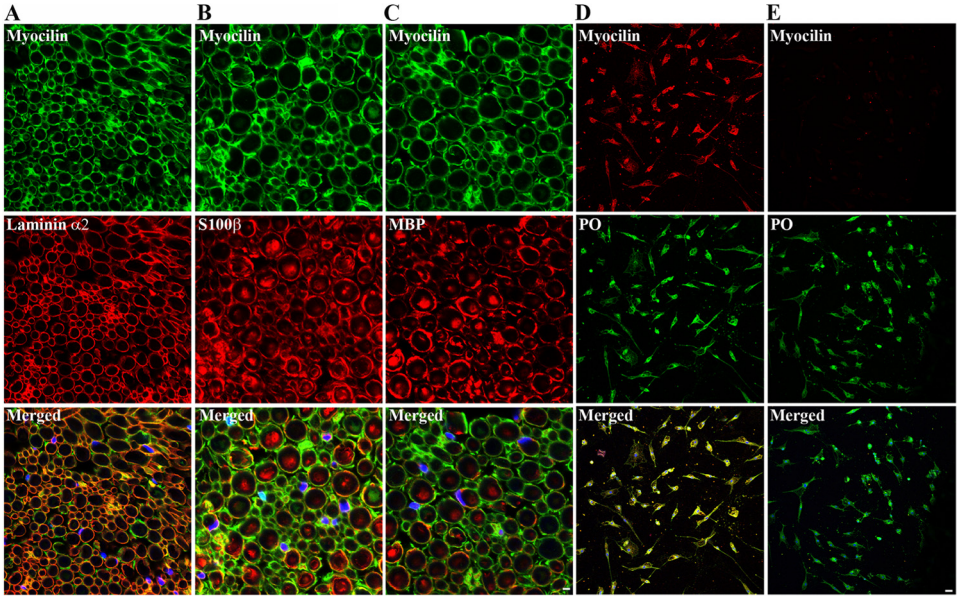

FIGURE 2. *A–C*, shown is localization of myocilin and Schwann cell-associated proteins in sciatic nerves of 6-month-old wild-type mice. Confocal images of isolated sciatic nerve transverse sections are shown. Sections were stained with antibodies against myocilin (1:500 dilution, *green*), laminin α2 (1:500 dilution, *red*, *A*), S100β (1:500 dilution, *red*, *B*), or MBP (1:500 dilution, *red*, *C*). Nuclei were stained with DAPI (*blue*). Myocilin partially co-localizes with Schwann cell markers. *Scale bar*,10 μm. *D* and *E*, confocal images of Schwann cells stained with antibodies against myocilin (1:500 dilution) and P0 (1:200 dilution). Nuclei were stained with DAPI (*blue*). Schwann cells were isolated from 5-day-old wild-type (*D*) or *Myoc* null (*E*) mice and cultured for 7 days. *Scale bar*, 10 μm.

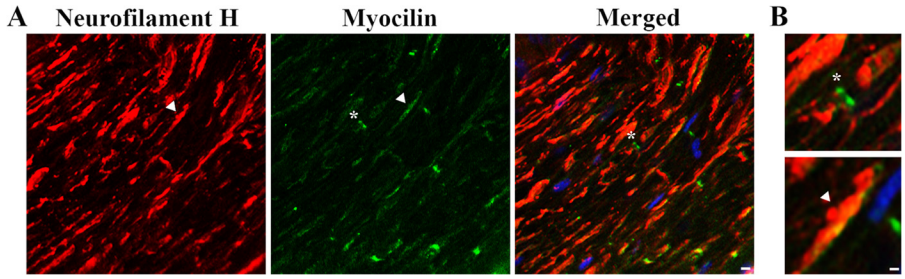

FIGURE 3. **Confocal images of 2-month-old mouse sciatic nerve in a longitudinal section.** Sections were stained with antibodies against myocilin (1:500 dilution, *green*) and neurofilament H (1:500 dilution, *red*). Nuclei were stained with DAPI (*blue*). *B* shows enlarged images marked with asterisks (*) and *white arrowheads* in *A*. *Scale bar*, 10 μm in *A* and 5 μm in *B*.

transmission electron microscope equipped with digital imaging capabilities. The g ratio was determined by dividing the circumference of an axon (without myelin) by the circumference of the same axon including myelin. Six wild-type and seven *Myoc* null mice were analyzed. 12 and 20 nodes were found and analyzed in the sciatic nerves of 5 wild-type and 12 *Myoc* null 2-month-old mice.

Phosphoreceptor Tyrosine Kinase Antibody Array—HEK293 cells grown on 25T flasks were treated with control or myocilin-containing medium for 30 min. Cells were lysed in the lysis buffer (20 mM Tris-HCl, pH 8.0, 137 mM NaCl, 10% glycerol, 2 mM EDTA, 1 mM sodium orthovanadate) containing a protease inhibitor mixture (Roche Applied Science). Equal amounts (200 μg) of cell lysates were added to human phosphoreceptor tyrosine kinase (RTK) antibody arrays containing 42 different anti-RTK antibodies (R&D systems, Minneapolis, MN). Information about anti-RTK antibodies spotted on the filters and the location of each spot can be found at the company's website. The antibody array was performed according to manufacturer's instructions. The signal was detected with Pierce ECL Western blotting Substrate by chemiluminescence. Intensities of identified spots were quantified using NIH ImageJ software.

Clustering—Clustering experiments were performed as described (23). In brief, DRG explants were cultured as above for 2 weeks on slides coated with 100 μg/ml poly-D-lysine and 10 μg/ml laminin (BD Biosciences). The neurons were then incubated with purified myocilin protein with or without anti-myocilin polyclonal antibody for 30 min, washed once with neurobasal medium, and grown for an additional 48 h in culture medium before fixing and staining. Quantification of nodal protein clustering was performed in three separate experiments by counting the number of NF186 and $Na_v1.2$ staining sites in several 320-μm square fields.

TUNEL Assay—The TUNEL assay was performed using the apoBrdU TUNEL assay kit (Invitrogen). Briefly, 1×10^4 isolated Schwann cells were seeded per well on two well chamber slides. Cells were washed in equilibration buffer, incubated with a TdT enzyme in a humidified chamber at 37 °C for 1 h, washed, and then incubated in the dark with fluorescein-488-conjugated anti-BrdU at room temperature for 30 min. The washed specimens were counterstained with DAPI, and images were collected using Zeiss LSM700 fluorescent confocal microscope.

Statistical Analysis—In the experiments where multiple samples were compared, statistical significance was determined using a one-way analysis of variance test.

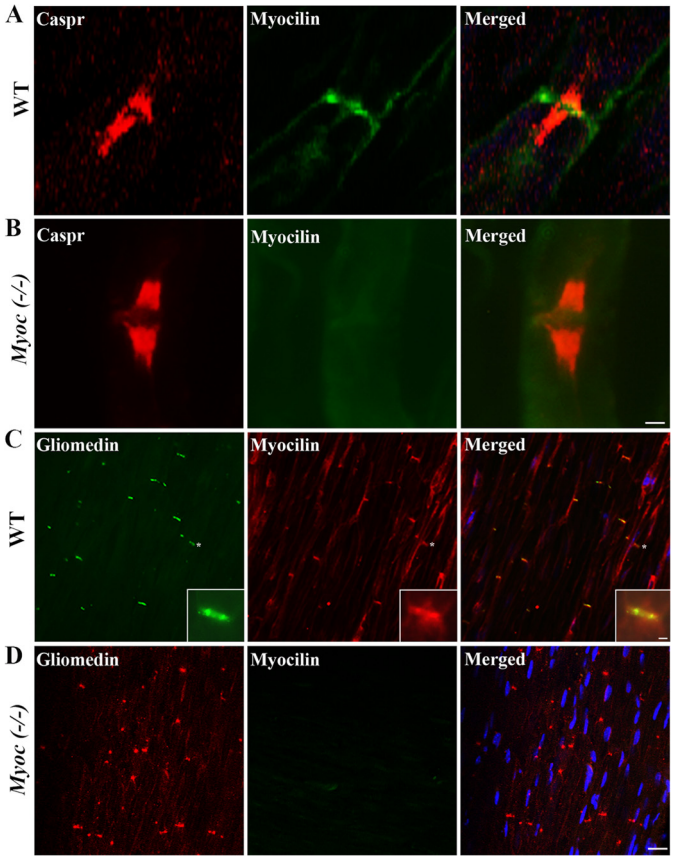

FIGURE 4. **Confocal images of 2-month-old wild-type (*A* and *C*) and *Myoc* null (*B* and *D*) mice sciatic nerves in longitudinal sections.** Sections were stained with antibodies against myocilin (1:500 dilution), caspr (1:200 dilution), and gliomedin (1:200 dilution). Nuclei were stained with DAPI (*blue*). *Insets* in *C* show higher magnification of the nodal region marked by *. Myocilin co-localizes with gliomedin at nodes of Ranvier. *Scale bars*: 5 μm in *A* and *B*; 20 μm in *C* and *D*; 2 μm in the *insets* in *C*.

RESULTS

Myocilin Interacts with Several Nodal Proteins within the Sciatic Nerve—Expression of the *Myoc* gene is reportedly detectable in rat sciatic nerve starting from P15 (13). We detected low levels of myocilin protein in mouse sciatic nerve as early as P3, the earliest analyzed stage, with expression levels increasing to reach approximately adult levels by P21, a time when myelination is almost completed (24) (Fig. 1). In transverse sections of adult mouse sciatic nerve, myocilin was detected mainly in Schwann cells as evidenced by co-localization of myocilin immunofluorescence with that of glial-associated proteins laminin α2, S100β, and MBP (Fig. 2, *A*–*C*). Cultured Schwann

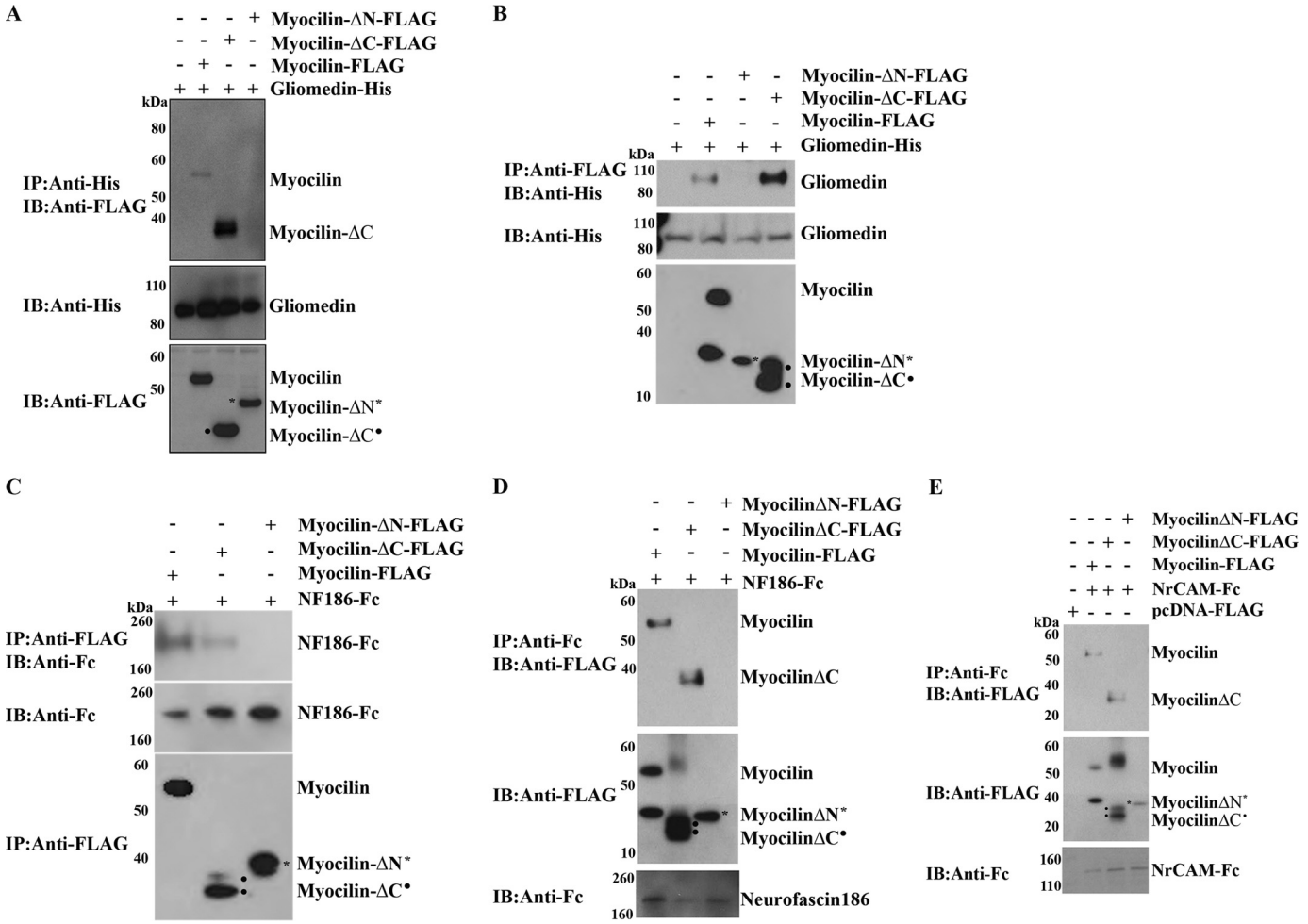

FIGURE 5. **Physical interaction of myocilin or its proteolytic fragments with gliomedin, neurofascin, and NrCAM.** HEK293 cells were co-transfected with the indicated constructs. CM was collected 48 h after transfection and treated with the indicated antibodies. After immunoprecipitation (*IP*), protein complexes were eluted from the beads, separated by SDS-PAGE, and probed with the indicated antibodies. *IB*, immunoblot. The *upper panels* show the results of immunoprecipitation. The *two lower panels* show the levels of tested proteins in CM before immunoprecipitation. 5% of CM used for immunoprecipitation was loaded. The myocilin-ΔC construct in many cases (see *panels B–E*) produced two well separated bands due to differential glycosylation. In some cases (see *panel A*), glycosylation was less pronounced). The *black dot* marks bands corresponding to Myocilin-ΔC; * marks bands corresponding to myocilin-ΔN.

cells isolated from P5 wild-type but not *Myoc* null mice also expressed myocilin (Fig. 2, *D* and *E*). Immunofluorescent labeling of longitudinal sections of sciatic nerve confirmed that myocilin was located preferentially in Schwann cells, with individual cells showing different intensity of staining. Because myocilin is a secreted protein interacting with NrCAM and NF186 (see below) that are expressed in neurons, partial overlapping of myocilin immunofluorescence with neuronal marker neurofilament H immunofluorescence was also observed (Fig. 3). Myocilin was concentrated at the nodes of Ranvier where it co-localized with gliomedin, a known nodal marker, but not with caspr, a known paranodal marker (Fig. 4*A* and *C*) (14). Specificity of myocilin immunostaining was confirmed using sciatic nerve from *Myoc* null mice that demonstrated the absence of myocilin staining, whereas gliomedin and caspr staining was not significantly disturbed (Fig. 4, *B* and *D*).

Co-localization of myocilin and gliomedin at sciatic nerve nodes of Ranvier prompted us to explore whether myocilin physically interacts with gliomedin and/or its receptors, NF186 and NrCAM. Myocilin can be proteolytically cleaved after Arg^{226}, resulting in two fragments of about 22- and 35-kDa molecular mass (25). Thus, we analyzed protein-protein interactions with full-length myocilin and its proteolytic fragments. Protein-protein interactions were first assessed using CM of transiently transfected HEK293 cells, as all constructs that we used encoded well secreted modified proteins (17, 19). Both myocilin and its N-terminal fragment (Myocilin-ΔC) but not the C-terminal fragment containing the olfactomedin domain (Myocilin-ΔN) interacted with gliomedin, NF186, and NrCAM (Fig. 5*A–E*). The N-terminal fragment of myocilin interacted more strongly with gliomedin than full-length myocilin (Fig. 5, *A* and *B*). Interaction of myocilin with neurofascin, NrCAM, and gliomedin in physiological conditions was confirmed using lysates of adult mouse sciatic nerve (Fig. 6). Nodal localization of myocilin and its interaction with several nodal proteins suggested that myocilin may play a role in the organization and/or function of the nodes of Ranvier in the sciatic nerve.

Sciatic Nerves of Myoc Null Mice Exhibit Myelin Abnormalities and Partially Disorganized Nodes of Ranvier—To explore whether the absence of myocilin affects the structural organization of the sciatic nerve, including the nodes of Ranvier, we

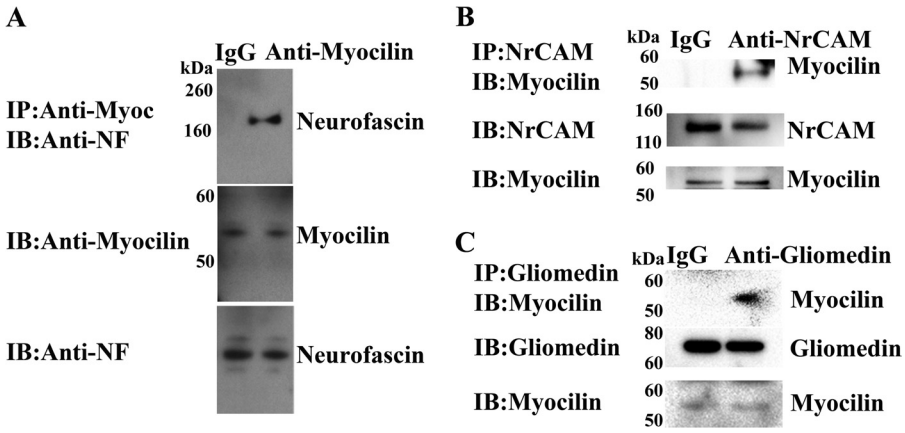

FIGURE 6. **Physical interaction of myocilin with neurofascin, NrCAM, and gliomedin.** Lysates of sciatic nerves were immunoprecipitated with the indicated antibodies. Immunoprecipitates (*IP*) were collected, separated by SDS-PAGE, and then probed with neurofascin (*NF*) or myocilin antibodies. Rabbit IgG was used as negative control. The *two lower panels* show the levels of tested proteins in lysates before immunoprecipitation. 5% of lysates used for immunoprecipitation were loaded. *IB*, immunoblot.

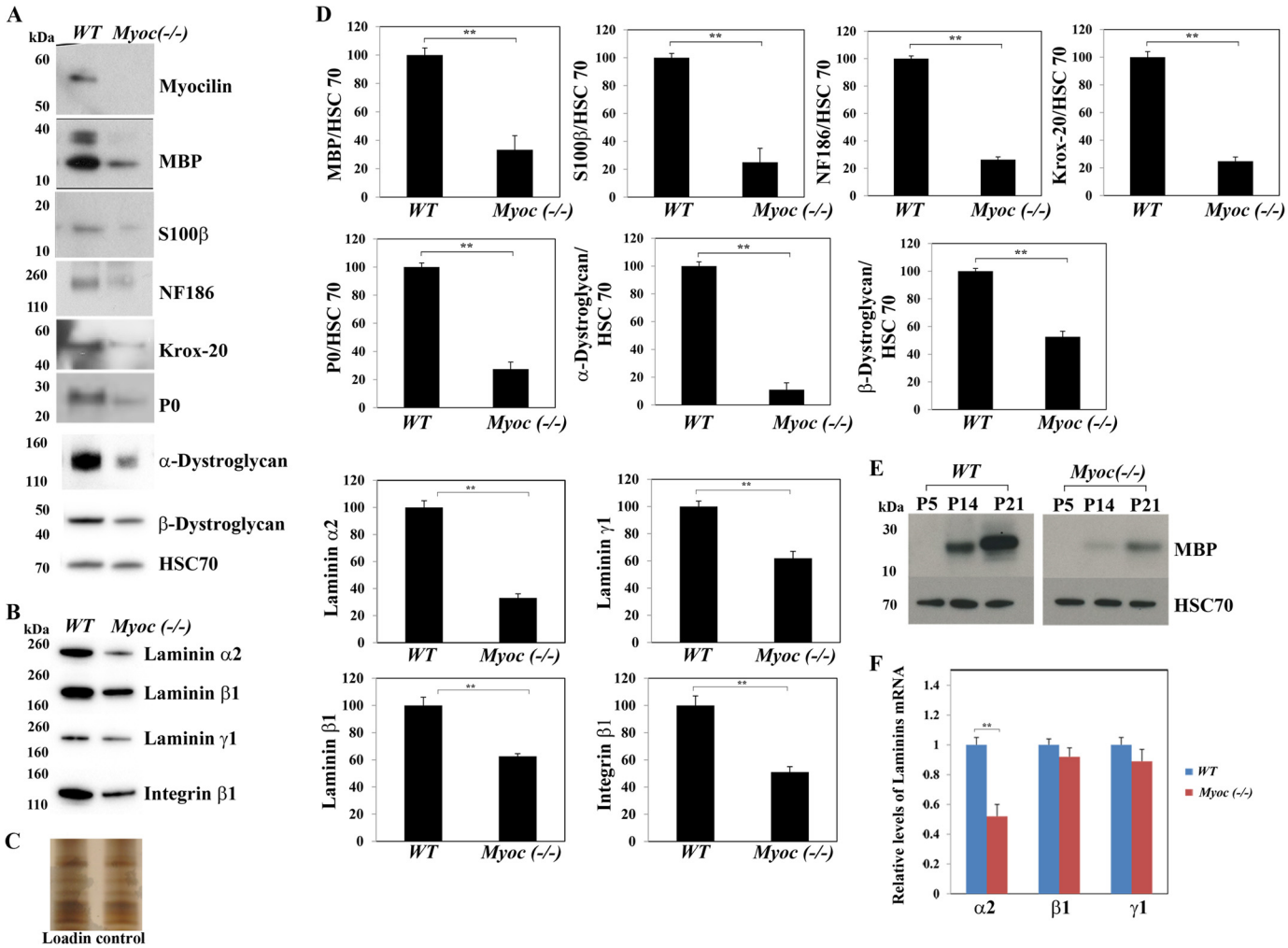

FIGURE 7. **Reduced levels of myelin proteins in the sciatic nerves of *Myoc* null mice.** *A*, Western blot analysis of sciatic nerve lysates of P25 *Myoc* null and wild-type littermates using myocilin (1:2,000 dilution), MBP (1:1,000 dilution), S100β (1:1,000 dilution), α-dystroglycan (1:1000 dilution), β-dystroglycan (1:1000 dilution), Krox-20 (1:1000 dilution), and NF186 (1:1000 dilution) antibodies is shown. Staining of the same blot with antibodies against HSC70 (1:5000 dilution) was used for normalization of loading. *B*, shown is Western blot analysis of sciatic nerve lysates of P22 *Myoc* null and wild-type littermates using laminin α2 (1:1000 dilution), laminin β1 (1:1000 dilution), laminin γ1 (1:1000 dilution), and integrin β1 (1:500 dilution) antibodies. *C*, shown is a silver-stained gel after separation of 8 M urea-soluble proteins that was used for normalization of Western blot in *B*. *D*, shown is quantification of three independent Western blot experiments as in (*A* and *B*). The levels of the corresponding proteins in sciatic nerve of wild-type mice were taken as 100% (*, $p < 0.05$; **, $p < 0.01$). Data are presented as the mean $\pm$ S.E. *E*, shown are MBP levels in the sciatic nerve lysates of wild-type and *Myoc* null mice of different ages (P5-P21) as judged by Western blot analysis. Staining of the same blot with antibodies against HSC70 (1:5000 dilution) was used for normalization of loading. *F*, shown are the relative levels of mRNAs encoding laminin chains in sciatic nerves of P22 mice as judged by real-time PCR. *GAPDH* mRNA was used for normalization The levels of corresponding mRNAs in sciatic nerve of wild-type mice were taken as 100% (**, $p < 0.01$). Data are presented as mean $\pm$ S.E.

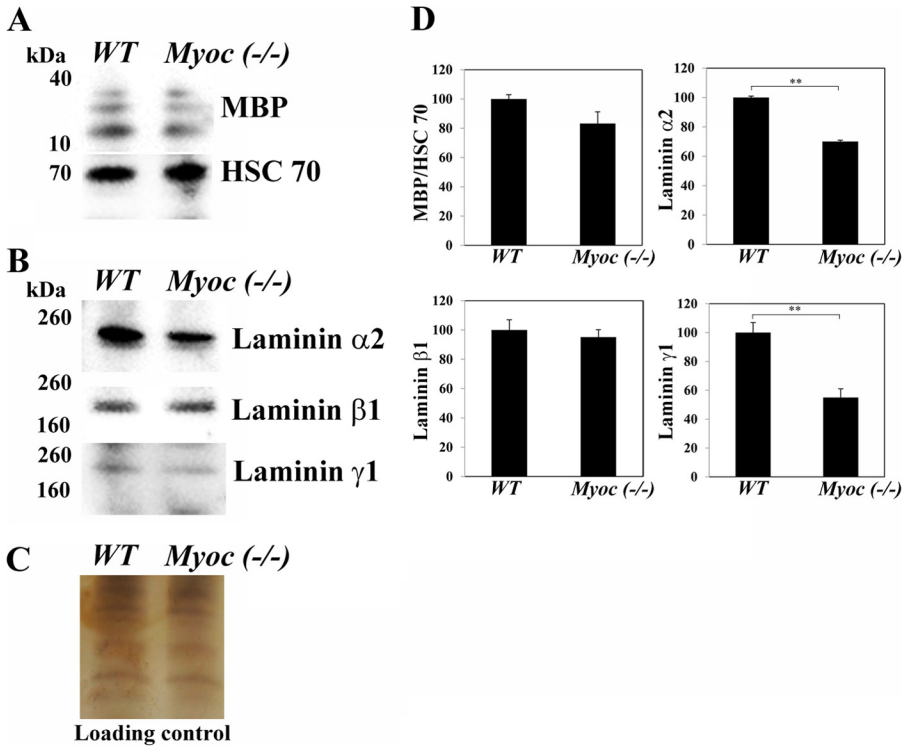

FIGURE 8. *A* and *B*, shown is Western blot analysis of sciatic nerve lysates of 3–5-month-old *Myoc* null and wild-type littermates using MBP (1:1000 dilution), laminin α2 (1:1000 dilution), laminin β1 (1:1000 dilution), and laminin γ1 (1:1000 dilution). Staining of the same blot with antibodies against HSC70 (1:5000 dilution) was used for normalization of loading for the MBP blot. *C*, shown is a silver-stained gel after separation of 8 M urea-soluble proteins that was used for normalization of Western blot for laminins. *D*, shown is quantification of three independent Western blot experiments as in (*A* and *B*). The levels of the corresponding proteins in sciatic nerve of wild-type mice were taken as 100%. **, $p < 0.01$. Data are presented as the mean ± S.E.

first evaluated the expression levels of several proteins by Western blotting and by immunofluorescence. Among the proteins tested, the overall levels of MBP, S100β, P0, laminin α2, laminin β1, laminin γ1, integrin β1, α-dystroglycan, β-dystroglycan, Krox-20, and NF186 were reduced in sciatic nerves of P22-P25 *Myoc* null mice compared with wild-type littermates (Fig. 7, *A–D*). Among laminin chains, laminin α2 was reduced more dramatically than laminin β1 and laminin γ1. At the mRNA level, only mRNA encoding laminin α2 was reduced in the sciatic nerve of *Myoc* null mice compared with wild-type samples, whereas the levels of laminin β1 and laminin γ1 mRNAs did not show statistically significant changes (Fig. 7*F*). Reduced levels of MBP, a major myelin component, were observed at different stages of sciatic nerve myelination (P14-P21) in *Myoc* null mice compared with wild type (Fig. 7*E*). In adult *Myoc* null and wild-type mice, the differences in the levels of MBP and tested laminin chains became less pronounced than in young animals, with only laminin α2 and γ1 chains showing statistically significant differences (Fig. 8).

Immunostaining of sciatic nerve sections confirmed the results of Western blot analysis; changes in the intensity of MBP staining between *Myoc* null and wild-type mice were more pronounced at early postnatal ages compared with adult animals, and the difference in the intensity of laminin α2 staining was more pronounced than such differences for β1 and γ laminins (Fig. 9, *A–D*).

It has been previously reported that laminin-deficient Schwann cells failed to radially sort and myelinate axons (26–28). Therefore, we compared myelination and sorting of axons in the sciatic nerves of wild-type and *Myoc* null mice. There were dysmyelinated areas in the sciatic nerves of 2-month-old *Myoc* null mice compared with wild-type animals (Fig. 10, *A* and *B*). In the dysmyelinated areas, unmyelinated axons were grouped in bundles in unsorted manner (*arrows* in Fig. 10, *A* and *B*). Immature Schwann cells were also observed with high frequency in *Myoc* null sciatic nerves (*arrowheads* in Fig. 10, *A* and *B*). Axons had a lower average diameter in the sciatic nerves of *Myoc* null mice compared with wild-type animals (Fig. 10*E*). In the subset of *Myoc* null Schwann cell/axon units that appeared to be relatively normal, the myelin sheaths were thinner, with lower electron density than those of wild-type mice (Fig. 10, *A–C*) with g ratios (inner axon diameter/total fiber diameter of myelinated axons) of 0.75 ± 0.01 ($n = 540$ *for Myoc* null) *versus* 0.63 ± 0.07 ($n = 350$ for wild-type) ($p < 0.01$) (Fig. 10*F*). The reduction in myelin thickness was observed in axons of different sizes ranging from 1 to 7 μm (Fig. 10*F*). Finally, the basal membrane of myelinated axons appeared fuzzy in most *Myoc* null samples and in some areas was disrupted as compared with the basal membrane in wild-type littermates (Fig. 10*D*). These differences may be connected with a lower density of membrane components in *Myoc* null mice.

Significant differences between wild-type and *Myoc* null mice were also observed in the nodal region. 20 and 12 nodes were analyzed by electron microscopy in *Myoc* null and wild-type nerve, respectively. Although all analyzed nodes in wild-type mice appeared morphologically normal, 15 of 20 analyzed nodes in *Myoc* null mice exhibited abnormalities of varying degrees (Fig. 11, *A–C*). Schwann cell microvilli normally have a

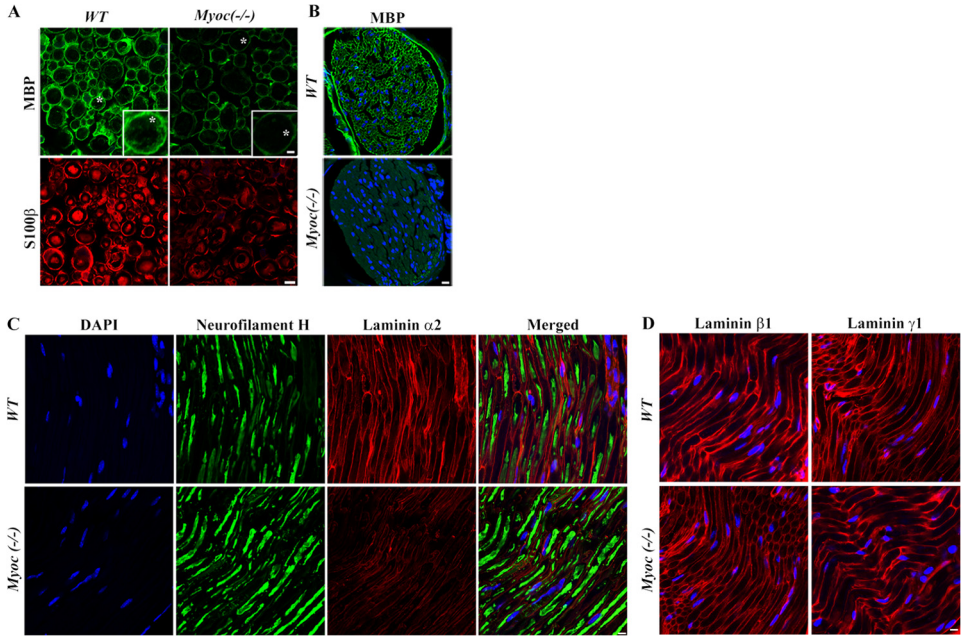

FIGURE 9. **Confocal images of wild-type and *Myoc* null adult.** *A*, shown are sciatic nerve cross-sections stained with MBP (1:500 dilution) and S100β (1:200 dilution). *Insets* (*low right corners*) show magnified images of areas marked by an *. *Scale bars*, 10 μm for the main images and 2 μm for enlarged inserts. *B*, shown are confocal images of wild-type and *Myoc* null P14 sciatic nerve cross-sections stained with MBP antibody (1:500 dilution). *Scale bar*, 20 μm. *C* and *D*, shown are confocal images of wild-type and *Myoc* P22 sciatic nerve cross-sections stained with antibodies against laminin α2 (1:200 dilution), laminin β1 (1:200 dilution), laminin γ1 (1:200 dilution), and neurofilament H (1:400 dilution). Nuclei were stained with DAPI (*blue*). *Scale bar*, 10 μm.

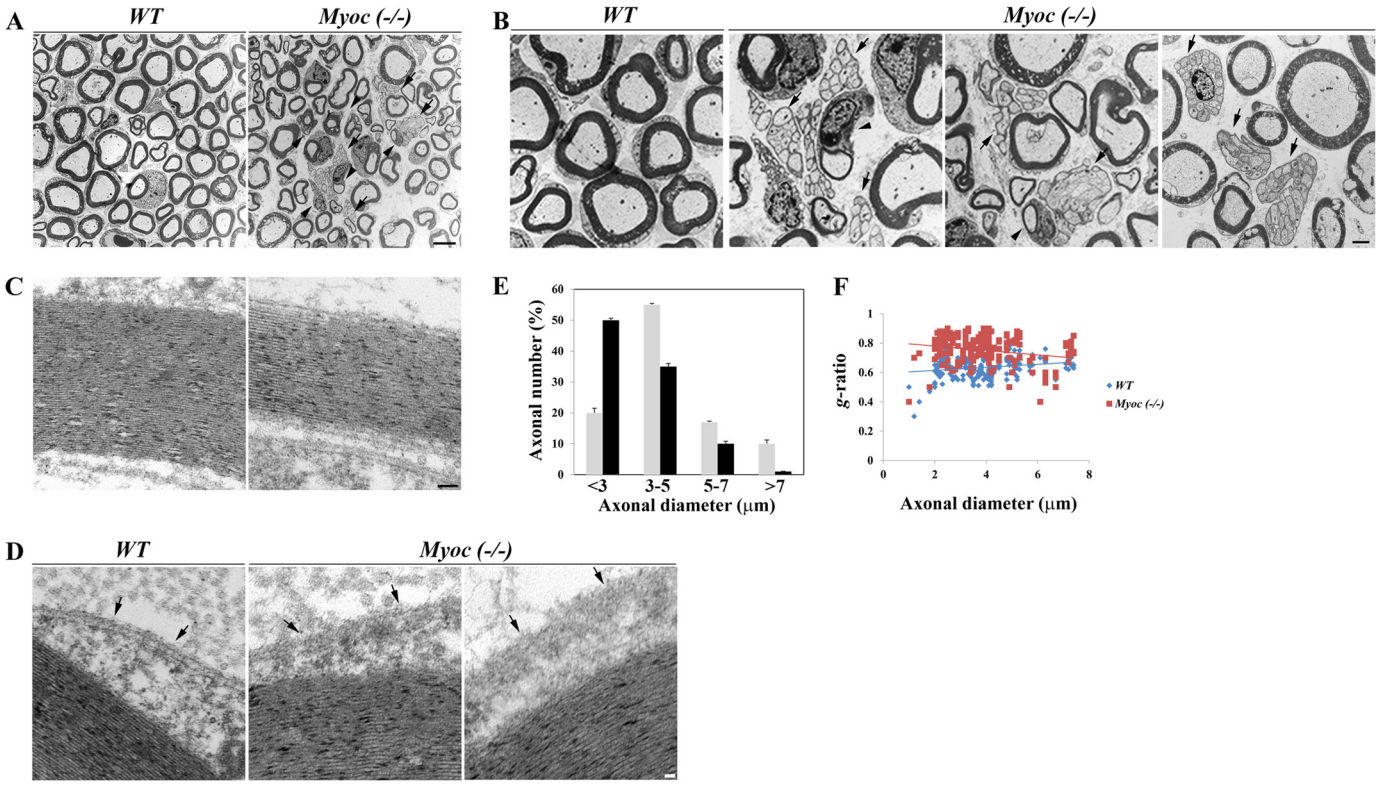

FIGURE 10. **Myoc null mice show defects in organization of sciatic nerves.** *A* and *B*, shown are electron micrographs of sciatic nerve cross-sections of 2-month-old wild-type and *Myoc* null mice. *Myoc* null mice showed a lower average axon diameter compared with wild-type animals. *Arrows* mark unmyelinated axons grouped in bundles in an unsorted manner, whereas *arrowheads* mark immature Schwann cells in *Myoc* null sciatic nerves. *Scale bars*, 10 μm in *A* and 5 μm in *B*. In the subset of *Myoc* null Schwann cell/axon units that appeared to be relatively normal, the myelin sheaths were thinner with lower electron density than those of wild-type mice. *C*, scale bar, 500 nm. *D*, basal membrane (*arrows*) very often (about 70% of length in 10 analyzed sciatic nerve samples) looked fuzzy compared with wild-type sciatic nerves. Typical images are shown. *Scale bar*, 5 μm. *E* and *F*, shown is the relative distribution of axon diameters and g ratios (axon diameter/fiber diameter of myelinated axons) for the sciatic nerve of wild-type and *Myoc* null mice. *Error bars* represent $\pm$ S.D.

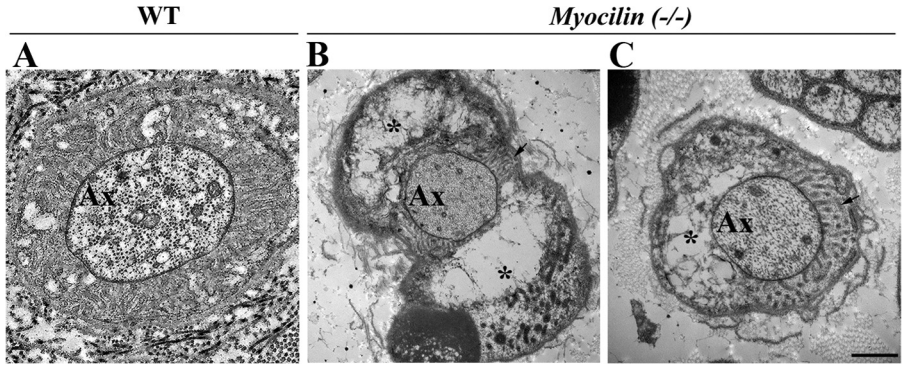

FIGURE 11. **Myoc null mice show defects in organization of Ranvier nodes.** Electron micrographs of sciatic nerves sectioned at nodes of 2 month-old wild-type (*A*) and *Myoc* null mice (*B* and *C*). Microvilli of Schwann cells normally have a relatively regular, radial arrangement around the centrally located axon. *A*, in the nodes of *Myoc* null mice, the microvilli often ran parallel to, or averted away from the axon (*arrows* in *B* and *C*). Degeneration of microvilli was also observed leading to the absence of microvilli in some areas (* in *B* and *C*). *Ax*, axons. *Scale bar*, 500 nm.

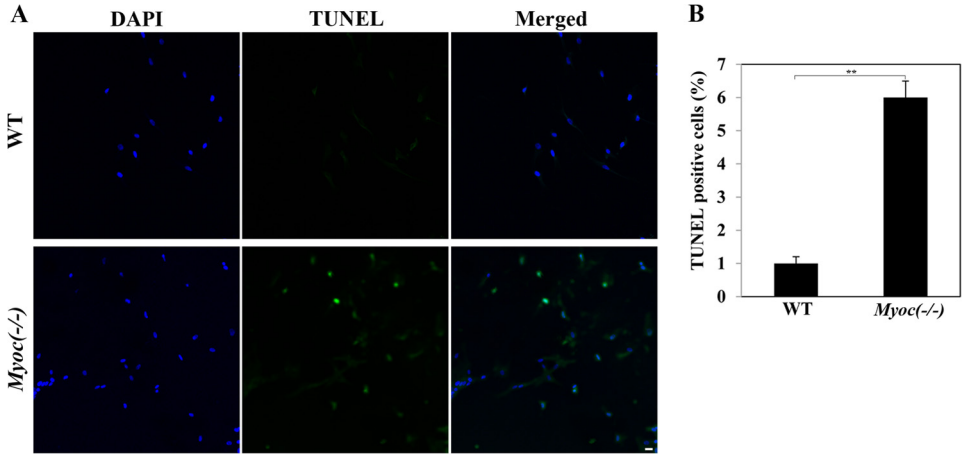

FIGURE 12. **Increased apoptosis in primary cultures of Schwann cells isolated from *Myoc* null mice.** *A*, shown are confocal images of Schwann cell cultures isolated from *Myoc* null and wild-type littermates after the TUNEL assay. *Scale bar*, 10 μm. *B*, shown is quantification of the results shown in *A*. **, $p < 0.01$. Data are presented as the mean ± S.E.

relatively regular, radial arrangement around the centrally located axon (Fig. 11A). In contrast, most of the nodes were partially disorganized in sciatic nerves of *Myoc* null mice (Fig. 11, *B* and *C*). The microvilli of *Myoc* null mice often ran parallel to, or averted away from, the axon, and their degeneration was observed in some areas (Fig. 11, *B* and C). It should be pointed out that Schwann cells isolated from *Myoc* null mice were more prone to apoptosis than those isolated from wild-type mice (Fig. 12). This may also contribute the degenerative processes observed in the nodes of *Myoc* null mice. In summary, our data suggest that myocilin might play an important role in sciatic nerve myelination and confirm its role in the organization and integrity of the nodes in the sciatic nerves.

Myocilin May Regulate Myelination through Epidermal Growth Factor Receptor Signaling—To identify the signaling pathway activated by myocilin, we employed human RTK antibody arrays. HEK293 cells were treated with control or myocilin-containing CM for 30 min and lysed. Equal amounts of lysates were added to the RTK antibody arrays, which were analyzed as suggested by the manufacturer. Among 42 different RTKs analyzed, only epidermal growth factor receptor (ErbB1) appeared activated by ~5-fold upon treatment with lysate from myocilin-treated cells compared with control cells (Fig. 13). It should be mentioned that ErbB2 and ErbB3 were also spotted at

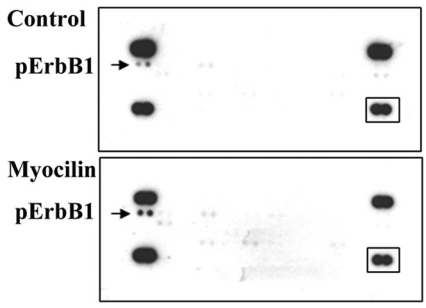

FIGURE 13. **Analysis of RTK phosphorylation.** Lysates of HEK293 cells treated with CM from control (*upper panel*) cells and cells expressing myocilin (*lower panel*) were added to human phospho-RTK antibody arrays. Arrays were treated as described under "Experimental Procedures." *Arrows* indicate spots corresponding to phosphorylated ErbB1 receptors on the blots. *Boxed spots* were used for normalization.

the RTK antibody arrays, but the level of their expression in HEK293 cells was very low compared with ErbB1 as judged by our gene expression array analysis (29).

It is now well established that signaling through ErbBs plays a critical role in myelination in the PNS (30, 31). There are four ErbBs in mammals. Available data suggest that ErbB1, ErbB2, and ErbB3 may be expressed at similar levels in adult mouse sciatic nerves, whereas ErbB4 is not expressed in the sciatic nerve (32, 33). In the sciatic nerve, ErbB2 and ErB3 are localized

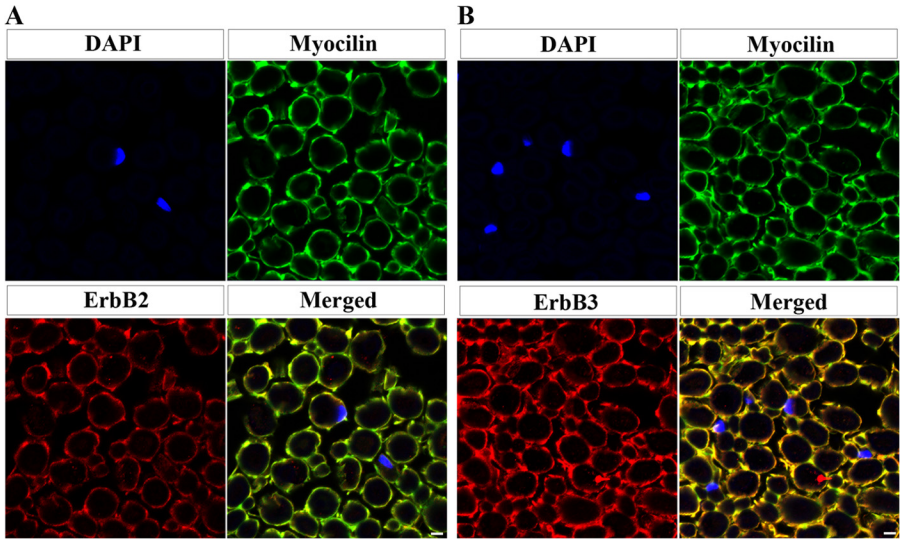

FIGURE 14. **Co-localization of myocilin with ErbB2 and ErbB3 in the mouse sciatic nerve.** Confocal images of 2-month-old wild-type sciatic nerve in cross-sections. Myocilin (in *green*) overlaps with ErbB2 (*red* in *A*) and ErbB3 (*red* in *B*). Nuclei were stained with DAPI (*blue*). *Scale bar*, 10 μm.

preferentially in Schwann cells (32, 33) with ErbB2 showing preferential localization to the nodal region of the myelinating Schwann cells, with individual cells showing different intensity of staining (34). These patterns of staining were very similar to the myocilin staining pattern that we observed (Figs. 2 and 4). Indeed, immunofluorescent labeling of sciatic nerve transverse sections with myocilin and ErbB2 or ErbB3 demonstrated co-localization of these proteins (Fig. 14, *A* and *B*).

To elucidate whether the defects in sciatic nerve myelination observed in *Myoc* null mice may be explained by modulation of ErbB signaling, we analyzed the effects of myocilin on ErbB signaling. It is known that heterodimers of ErbB2 and ErbB3 are critical for Schwann cell differentiation (35), so our analysis focused on these receptors. First, we sought to determine whether myocilin physically interacts with ErbB2/ErbB3 complexes. NIH3T3 cells were transfected with various receptor constructs and then treated with CM from cells expressing myocilin fused to AP or CM from cells expressing free AP (19). Myocilin bound stronger to cells expressing both ErbB2 and ErbB3 than to cells expressing either ErbB2 or ErbB3 alone (Fig. 15*A*). The affinities of myocilin for ErbB2, ErbB3, and their combination were estimated by measuring binding levels of increasing concentrations of the myocilin-AP protein to ErbB-expressing COS7 cells. The calculated K_d were 27.8 $\pm$ 0.4, 23.7 $\pm$ 0.7, and 17.3 $\pm$ 0.2 nM for ErbB2, ErbB3, and their combination, respectively (Fig. 15, *B–D*). *In vivo* binding of myocilin to ErbB2 and ErbB3 was confirmed by immunoprecipitation using sciatic nerve extracts (Fig. 15, *E–H*). Phosphorylation of ErbB2 at Tyr-1221 was diminished in sciatic nerves of *Myoc* null mice and increased in transgenic mice expressing elevated levels of myocilin compared with wild-type mice, although the total levels of ErbB2 were similar in the sciatic nerves of these lines (Fig. 15, *I–J*). Several major signaling pathways are stimulated upon activation of ErbB2/ErbB3. We tested whether reduced ErbB2 phosphorylation in *Myoc* null mice is associated with attenuated activation of one of such pathway, PI3K-AKT. Among proteins tested, the levels of PI3Kβ and p-AKT were reduced in *Myoc* null mice compared with wild-type littermates, whereas the levels of PI3Kα and PI3K regulatory subunit p85 did not change (Fig. 16, *A* and *B*). PI3K activity is antagonized by PTEN (36), which inhibits myelination in Schwann cells together with Dlg1 (37). The levels of both Dlg1 and PTEN were increased in sciatic nerve of *Myoc* null mice compared with wild-type littermates (Fig. 16, *A* and *B*). On the basis of these results, we concluded that myocilin is able to signal through ErbBs, and this signaling may be related to myelination in the sciatic nerve.

Myocilin Induces Clustering of Nodal Components—Because myocilin interacts with several nodal components, we evaluated whether myocilin, similar to gliomedin (14), induces clustering of nodal proteins in isolated DRG explant cultures. DRGs, which had been permitted to regenerate axons for 5 days, were treated with myocilin for 30 min at room temperature, washed with basal media, and then incubated for an additional 24 h at 37 °C. This treatment resulted in axonal clustering of NF186 and sodium channel $Na_v1.2$ (Fig. 17, *A–F*). Myocilin co-localized with >80% of NF186 clusters ($p < 0.01$). Preincubation of myocilin with polyclonal antibody against myocilin for 30 min at room temperature before DRG exposure significantly reduced the clustering effect of myocilin (Fig. 17, *B* and *F*). Myocilin-induced clustering of nodal components requires signaling through ErbB1 and ErbB2, as the addition of GW2974, a dual inhibitor of these receptor tyrosine kinases, dramatically reduced the clustering effect of myocilin (Fig. 17*D*). We concluded that myocilin, similar to gliomedin, induces clustering of nodal components and that signaling through ErbB receptors contributes to this process.

DISCUSSION

Although a connection between mutations in the *MYOC* gene and glaucoma is well established, the role of wild-type myocilin is poorly understood. Our recent observations indicate that myocilin plays a role in several non-ocular tissues including skeletal muscle (10). In skeletal muscle, myocilin interacts with α-syntrophin and is part of the dystrophin-associated protein complex. Overexpression of myocilin in trans-

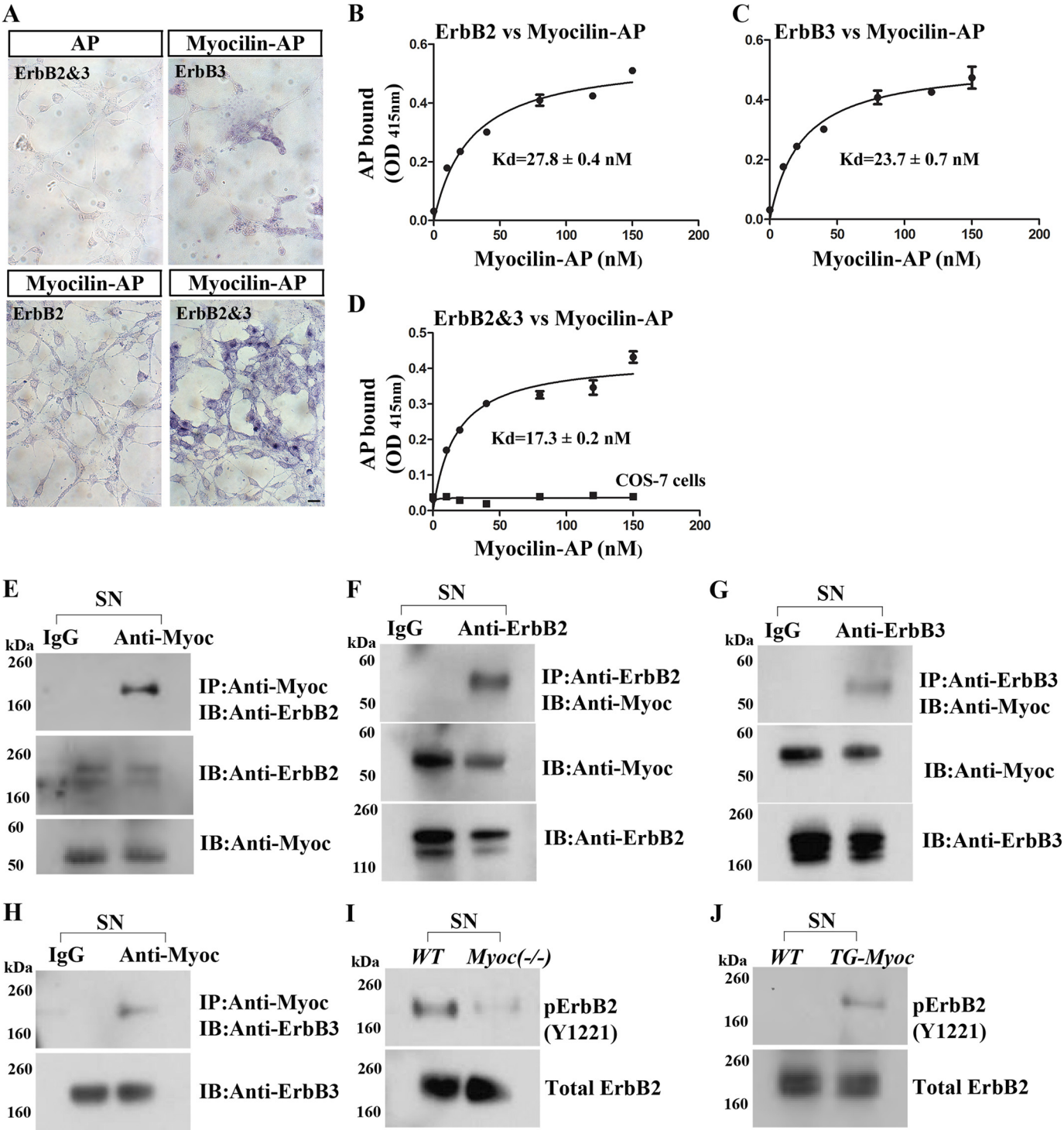

FIGURE 15. **Myocilin signaling through ErbB2/ErbB3 complex.** *A*, shown is binding of myocilin-AP to ErbB2/ErbB3. Myocilin-AP CM (2 nM) was incubated with NIH3T3 cells transfected with indicated ErbB constructs. The AP activity was visualized by staining with nitro blue tetrazolim/5-bromo-4-chloro-3-indolyl phosphate. CM from cells expressing AP was used as a control. *Scale bar*, 10 μm. *B–D*, Scatchard plots of myocilin-AP binding to ErbB2, ErbB3, and their combination are shown. Measurements were done in triplicate. *Error bars* represent ± S.D. *E–H*, co-immunoprecipitation of myocilin with ErbB2 and ErbB3 from the extracts of sciatic nerves (*SN*) is shown. Extracts were treated with antibodies against myocilin (1:1000 dilution), ErbB2 (1:1000 dilution), or ErbB3 (1:1000 dilution), and protein complexes were immunoprecipitated (*IP*) using protein G beads, eluted from the beads, separated by SDS-PAGE, and then probed with antibodies against ErbB2, ErbB3, or myocilin (1:1000). Immunoprecipitation with rabbit IgG was used as a control. The *lower panel* shows Western blot (*IB*) of lysates (10% input) before immunoprecipitation. *I* and *J*, ErbB2 phosphorylation in the sciatic nerves of wild-type, *Myoc* knock-out, and *Myoc* transgenic mice is shown. Note that larger amount of total protein was loaded, and longer exposure was used in *I* to detect phosphorylation of ErbB2 in *Myoc* null mice.

genic mice leads to a redistribution of some proteins in the complex and increases its stability. In particular, the level of the active form of α-dystroglycan and laminin binding to α-dystroglycan were markedly increased in muscle of transgenic mice as compared with wild-type littermates. Conversely, *Myoc* null mice demonstrated a moderate reduction in the amount of syn-

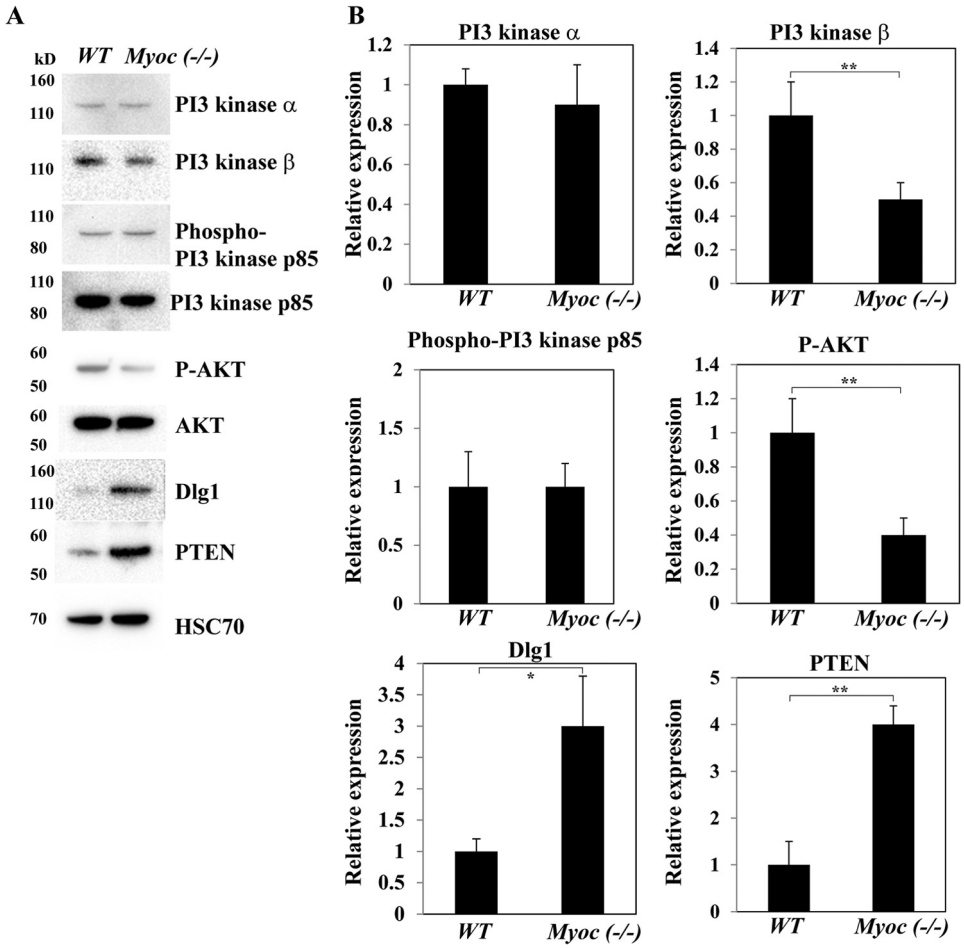

FIGURE 16. **Western blot analysis of the components of the PI3K pathway.** *A*, lysates of sciatic nerves from 1-month-old *Myoc* null or wild-type littermates were probed with the indicated antibodies. Staining with antibodies against HSC70 was used for normalization of loading. *B*, shown is quantification of three independent Western blot experiments as in *A*. The levels of corresponding proteins in sciatic nerve of wild-type mice were taken as one arbitrary unit (*, $p < 0.05$; **, $p < 0.01$). Data are presented as the mean ± S.E.

trophin associated with dystrophin compared with wild-type littermates, which led to a reduction in the level of the active form of α-dystroglycan (10). Although we did not perform careful morphological or behavioral studies, adult *Myoc* null mice were viable, fertile, and did not demonstrate visible abnormalities including gross tremor (8, 10).

Here we demonstrate that myocilin is involved in sciatic nerve myelination, interacts with and induces clustering of several nodal proteins, and participates in nodal integrity in the PNS. In the sciatic nerve, myocilin is actively expressed in Schwann cells but not in neurons. The absence of myocilin expression in axons reported here together with published results (13) argues against the idea that a reduced average diameter of axons in the sciatic nerve of *Myoc* null mice compared with wild-type littermates can be explained by neuron-autonomous effects of myocilin loss of function. Another olfactomedin domain-containing protein, gliomedin, has also been detected at PNS nodes where it was concentrated in Schwann cell microvilli (14). Unlike myocilin, which is secreted, gliomedin is a membrane-bound protein. However, the extracellular portion of gliomedin containing the olfactomedin domain may be cleaved in a furin-dependent manner and released into the extracellular space (17). Myocilin co-localizes with gliomedin in the nodal region of sciatic nerves and interacts with gliomedin via the N-terminal domain of myocilin that lacks the olfactomedin domain. Similar to gliomedin, myocilin interacts with NF186 and NrCAM and induces clustering of neurofascin and sodium channels in cultured dorsal root ganglion neurons in the absence of myelinating cells. Our data suggest that myocilin interacts with gliomedin, NF186, and NrCAM directly, but we cannot exclude a possibility that other unidentified proteins are necessary for such interactions and protein complex formation. The genetic elimination of gliomedin (16) similar to genetic elimination of myocilin (8) does not lead to abnormal gross phenotypes. We suggest that myocilin and gliomedin may perform complimentary functions in the PNS, although the effects of knocking out myocilin appear to be more severe than for gliomedin. It has been demonstrated that gliomedin null mice display no overt neurological abnormalities and exhibit normal nerve conduction. These mice formed compact PNS myelin that was indistinguishable from their wild-type littermates but exhibited disorganization and impaired attachment of Schwann cell microvilli to the nodal axolemma (16). It has been proposed that Schwann cells govern the assembly of PNS nodes by two overlapping independent processes that cooperate to provide reciprocal backup systems to ensure fast conduc-

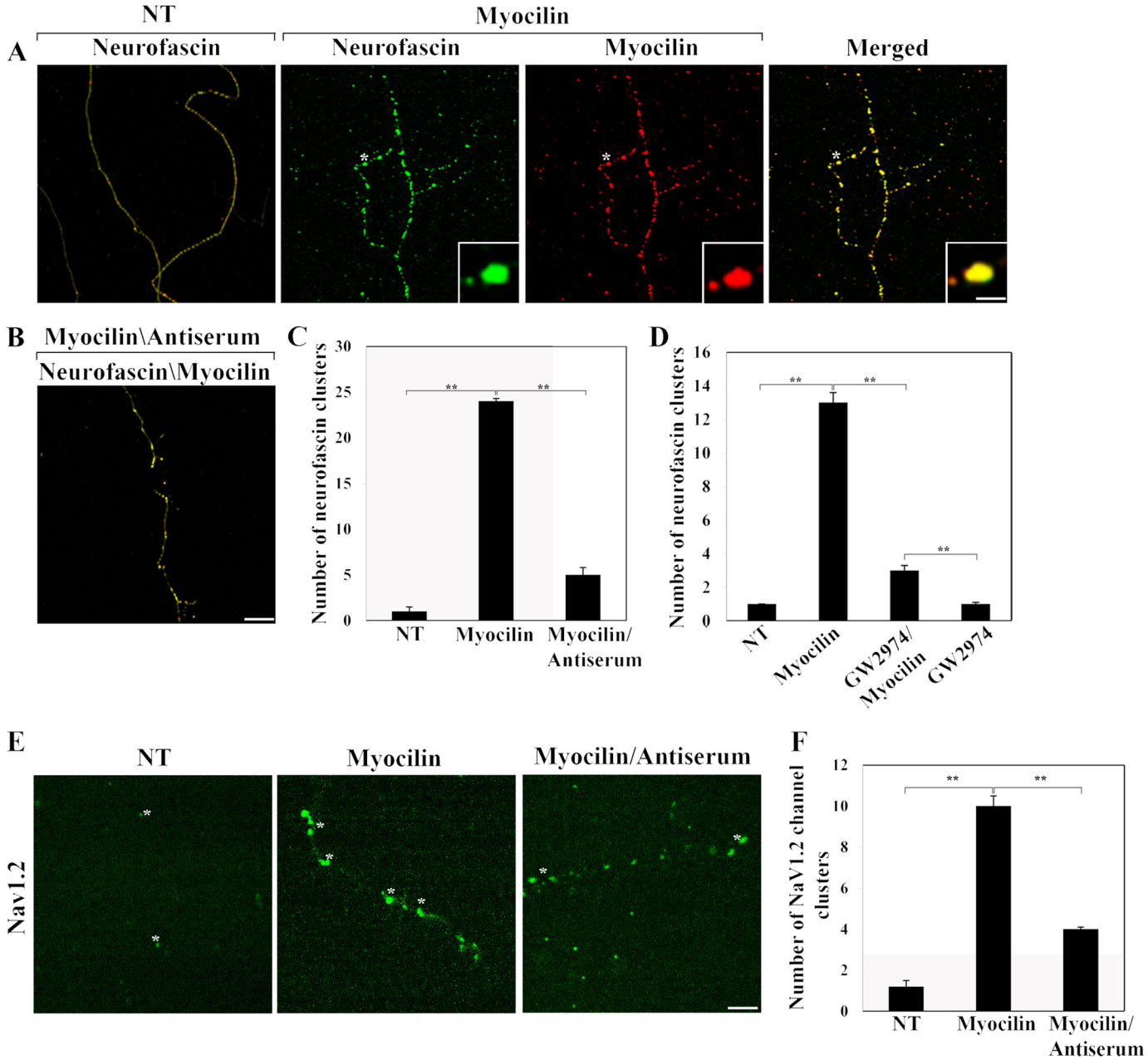

FIGURE 17. **Myocilin induces clustering of neurofascin and $Na_v1.2$ when added to DRG.** *A*, shown is clustering of neurofascin after the addition of myocilin. DRG neurons were treated with myocilin (3 μg/ml) for 30 min at 23 °C, washed with PBS, and then incubated for additional 24 h at 37 °C. Subsequently, DRG cultures were fixed and immunostained with antibodies against neurofascin and myocilin. The *inset* shows magnified images of areas marked by *. *NT*, no myocilin was added. *Scale bars*, 10 μm for the main images and 1 μm for the inset. *B*, shown is preincubation of myocilin with antibodies against myocilin for 30 min at room temperature before the addition to DRG significantly reduced clustering effect of myocilin. *C*, shown is quantification of three independent experiments investigating myocilin effects on clustering of neurofascin. Myocilin and antiserum against myocilin were added as in *B*. *D*, shown are the effects of inhibitor of ErbB1/ErbB2 kinases, GW2974, on myocilin-induced clustering of neurofascin. GW2974 was added in final concentration of 2.5 μM to culture medium ($n = 3$; **, $p < 0.01$). *Error bars* represent ± S.D. *E*, shown is clustering of $Na_v1.2$ after the addition of myocilin and myocilin together with antiserum as in *A* and *B*. *Scale bar*, 10 μm. *F*, shown is quantification of three independent experiments investigating myocilin effects on clustering of $Na_v1.2$.

tion in myelinated nerves (16). Here we show that sciatic nerves of *Myoc* null mice have reduced levels of several myelin and basement membrane proteins including MBP, P0, and laminin 2 (α2, β1, and γ1 chains), thinner myelin sheaths, defective radial sorting of axons, and abnormal nodes of Ranvier when compared with wild-type littermates. We speculate that, similar to skeletal muscle, elimination of myocilin leads to a reduced stability of the dystrophin glycoprotein complex in Schwann cells (38), resulting in reduced levels of α- and β-dystroglycans (Fig. 7, *A* and *B*). It has been previously shown that specific ablation of dystroglycan in Schwann cells led to profound nodal changes including reduced sodium channel density and disorganized microvilli (39). At the same time, the sciatic nerve of dystroglycan null mice did not show a significant reduction in the levels of laminin α2, β1, and γ1 chains compared with wild-type mice (39). Therefore, reduced levels of laminin α2, laminin β1, and laminin γ1 in *Myoc* null sciatic nerve compared with wild-type samples cannot be explained solely by the reduction

in the levels of their dystroglycan receptor. Changes in the laminin 2 level may contribute to the observed defects in the axon myelination and Schwann cell differentiation in *Myoc* null mice (Figs. 10 and 11). It has been shown that Schwann cell-specific ablation of laminin γ1 resulted in depletion of all other laminin chains in these cells. At P28, mutant sciatic nerve showed large bundles of unsorted axons with some Schwann cells located outside of axon bundles. Mutant Schwann cells lacked a continuous basal lamina (27). These defects were more severe than those observed in *dy2J/dy2J* or *dy3K/dy3K* mutants (27, 40). Null mutation of laminin α2 chain in *dy3K/dy3K* mice resulted in elevated levels of laminin α4 chain, a component of laminin-8, in the sciatic nerve, which can partially compensate for the loss of laminin-2 (40). At the same time, mice hypomorphic for laminin γ1 subunit expression demonstrated Schwann cell axonal sorting defects and continuous basal membranes with reduced levels of structural components (41). Defects in axon myelination in the sciatic nerve of *Myoc* null mice were less dramatic than the ones that were observed in the sciatic nerve after ablation of individual laminin chains and were more similar to ones observed in mice hypomorphic for laminin γ1. It is also interesting to note that hindlimb muscle mass was gradually reduced in laminin γ1 hypomorphic mice (41). Although we did not carefully analyze hindlimb muscle in *Myoc* null mice, we previously reported that overexpression of myocilin in hindlimbs led to an increase of their mass and average size of muscle fibers (10).

In the PNS, axon-derived factor neuregulin 1 (Nrg1) is one of the key factors regulating myelination (33, 42). Nrg1 acts by activating a family of tyrosine kinase ErbBs. ErbB1 binds Nrg1 only after dimerization with ErbB4. ErbB2 does not bind Nrg1 or any known ligand with high affinity but is able to transmit the Nrg1 signal after dimerization with ErbB3 or ErbB4. ErbB3 lacks tyrosine kinase activity and transmits signals only after dimerization with ErbB2. Among homodimers, only ErbB4 dimers are able to transmit Nrg1 signals. Our data demonstrate that myocilin may also signal through the ErbB family. Because the level of ErbB4 is very low in sciatic nerve, we studied the interaction of myocilin with ErbB2-3. Similar to Nrg1, myocilin binds ErbB2/ErbB3 heterodimers, but unlike Nrg1 it also binds ErbB2 alone. K_D values for myocilin binding to ErbB3 or ErbB2/ErbB3 complex were higher than the corresponding reported values for Nrg1; reported K_D values for Nrg1 binding to COS7 cells transfected with ErbB3 ranged from 1.9 to 11 nM (43, 44). Myocilin binding leads to the activation of ErbB signaling as evident by the phosphorylation of Tyr-1221 in ErbB2. At present, we do not know whether myocilin competes with Nrg1 for binding to the same sites in ErbBs. Disruption of Nrg1 of Nrg1 or its receptors (ErbB2/ErbB3) leads to the nearly complete loss of Schwann cells followed by the death of motor and sensory neurons that they support (45–48), whereas disruption of *Myoc* by null mutation reduces myelination but does not eliminate Schwann cells. Nevertheless, cultured *Myoc* null Schwann cells are more prone to apoptosis than those isolated from wild-type mice. It has been reported that laminin knock-out reduces phosphorylation of ErbB receptors in Schwann cells (27). In *Myoc* null mice, although decreased levels of laminins may contribute to a reduced phosphorylation of ErbB2, the reduction of laminin levels results from myocilin elimination. Moreover, overexpression of myocilin in transgenic mice led to an elevated phosphorylation of ErbB2 (Fig. 15*J*), supporting a primary role of myocilin in the regulation of ErbB signaling. It has been reported that disruption of neurofascin and gliomedin at nodes of Ranvier precedes demyelination in experimental allergic neuritis (49). These alterations correlated with the presence of serum antibodies against neurofascin and gliomedin suggest that autoantibodies against nodal proteins might contribute to disease progression in inflammatory demyelinating pathologies (49). It would be interesting to investigate whether similar changes occur with myocilin in patients with peripheral neuritis and various neuropathies. It would be also useful to test possible functional and structural defects in PNS of people with *MYOC*-related glaucoma, as these patients have not been systematically tested. Previously, we demonstrated that myocilin may serve as a modulator of the Wnt signaling pathway (19). Here we show that myocilin may modulate ErbB signaling. Our data introduce myocilin as a novel player in sciatic nerve myelination and suggest that myocilin is a multifunctional protein that may have differing functions in ocular and non-ocular tissues.

REFERENCES

1. Tomarev, S. I., and Nakaya, N. (2009) Olfactomedin domain-containing proteins. Possible mechanisms of action and functions in normal development and pathology. *Mol. Neurobiol.* **40,** 122–138
2. Fingert, J. H., Héon, E., Liebmann, J. M., Yamamoto, T., Craig, J. E., Rait, J., Kawase, K., Hoh, S. T., Buys, Y. M., Dickinson, J., Hockey, R. R., Williams-Lyn, D., Trope, G., Kitazawa, Y., Ritch, R., Mackey, D. A., Alward, W. L., Sheffield, V. C., Stone, E. M. (1999) Analysis of myocilin mutations in 1703 glaucoma patients from five different populations. *Hum. Mol. Genet.* **8,** 899–905
3. Fingert, J. H., Stone, E. M., Sheffield, V. C., and Alward, W. L. (2002) Myocilin glaucoma. *Surv. Ophthalmol.* **47,** 547–561
4. Stone, E. M., Fingert, J. H., Alward, W. L., Nguyen, T. D., Polansky, J. R., Sunden, S. L., Nishimura, D., Clark, A. F., Nystuen, A., Nichols, B. E., Mackey, D. A., Ritch, R., Kalenak, J. W., Craven, E. R., and Sheffield, V. C. (1997) Identification of a gene that causes primary open angle glaucoma. *Science* **275,** 668–670
5. Kwon, Y. H., Fingert, J. H., Kuehn, M. H., and Alward, W. L. (2009) Primary open-angle glaucoma. *N. Engl. J. Med.* **360,** 1113–1124
6. Adam, M. F., Belmouden, A., Binisti, P., Brézin, A. P., Valtot, F., Béchetoille, A., Dascotte, J. C., Copin, B., Gomez, L., Chaventré, A., Bach, J. F., and Garchon, H. J. (1997) Recurrent mutations in a single exon encoding the evolutionarily conserved olfactomedin-homology domain of TIGR in familial open-angle glaucoma. *Hum. Mol. Genet.* **6,** 2091–2097
7. Lam, D. S., Leung, Y. F., Chua, J. K., Baum, L., Fan, D. S., Choy, K. W., and Pang, C. P. (2000) Truncations in the TIGR gene in individuals with and without primary open-angle glaucoma. *Invest. Ophthalmol. Vis. Sci.* **41,** 1386–1391
8. Kim, B. S., Savinova, O. V., Reedy, M. V., Martin, J., Lun, Y., Gan, L., Smith, R. S., Tomarev, S. I., John, S. W., and Johnson, R. L. (2001) Targeted disruption of the myocilin gene (Myoc) suggests that human glaucoma-causing mutations are gain of function. *Mol. Cell. Biol.* **21,** 7707–7713
9. Wiggs, J. L., and Vollrath, D. (2001) Molecular and clinical evaluation of a patient hemizygous for TIGR/MYOC. *Arch. Ophthalmol.* **119,** 1674–1678
10. Joe, M. K., Kee, C., and Tomarev, S. I. (2012) Myocilin interacts with syntrophins and is member of dystrophin-associated protein complex. *J. Biol. Chem.* **287,** 13216–13227
11. Tomarev, S. I., Tamm, E. R., and Chang, B. (1998) Characterization of the mouse Myoc/Tigr gene. *Biochem. Biophys. Res. Commun.* **245,** 887–893
12. Torrado, M., Trivedi, R., Zinovieva, R., Karavanova, I., and Tomarev, S. I.

(2002) Optimedin. A novel olfactomedin-related protein that interacts with myocilin. *Hum. Mol. Genet.* **11,** 1291–1301
13. Ohlmann, A., Goldwich, A., Flügel-Koch, C., Fuchs, A. V., Schwager, K., and Tamm, E. R. (2003) Secreted glycoprotein myocilin is a component of the myelin sheath in peripheral nerves. *Glia* **43,** 128–140
14. Eshed, Y., Feinberg, K., Poliak, S., Sabanay, H., Sarig-Nadir, O., Spiegel, I., Bermingham, J. R., Jr., and Peles, E. (2005) Gliomedin mediates Schwann cell-axon interaction and the molecular assembly of the nodes of Ranvier. *Neuron* **47,** 215–229
15. Eshed, Y., Feinberg, K., Carey, D. J., and Peles, E. (2007) Secreted gliomedin is a perinodal matrix component of peripheral nerves. *J. Cell Biol.* **177,** 551–562
16. Feinberg, K., Eshed-Eisenbach, Y., Frechter, S., Amor, V., Salomon, D., Sabanay, H., Dupree, J. L., Grumet, M., Brophy, P. J., Shrager, P., and Peles, E. (2010) A glial signal consisting of gliomedin and NrCAM clusters axonal Na^+ channels during the formation of nodes of Ranvier. *Neuron* **65,** 490–502
17. Maertens, B., Hopkins, D., Franzke, C. W., Keene, D. R., Bruckner-Tuderman, L., Greenspan, D. S., and Koch, M. (2007) Cleavage and oligomerization of gliomedin, a transmembrane collagen required for node of ranvier formation. *J. Biol. Chem.* **282,** 10647–10659
18. Gould, D. B., Miceli-Libby, L., Savinova, O. V., Torrado, M., Tomarev, S. I., Smith, R. S., and John, S. W. (2004) Genetically increasing Myoc expression supports a necessary pathologic role of abnormal proteins in glaucoma. *Mol. Cell. Biol.* **24,** 9019–9025
19. Kwon, H. S., Lee, H. S., Ji, Y., Rubin, J. S., and Tomarev, S. I. (2009) Myocilin is a modulator of Wnt signaling. *Mol. Cell. Biol.* **29,** 2139–2154
20. Malyukova, I., Lee, H. S., Fariss, R. N., and Tomarev, S. I. (2006) Mutated mouse and human myocilins have similar properties and do not block general secretory pathway. *Invest. Ophthalmol. Vis. Sci.* **47,** 206–212
21. Poliak, S., Salomon, D., Elhanany, H., Sabanay, H., Kiernan, B., Pevny, L., Stewart, C. L., Xu, X., Chiu, S. Y., Shrager, P., Furley, A. J., and Peles, E. (2003) Juxtaparanodal clustering of Shaker-like K^+ channels in myelinated axons depends on Caspr2 and TAG-1. *J. Cell Biol.* **162,** 1149–1160
22. Porter, S., Clark, M. B., Glaser, L., and Bunge, R. P. (1986) Schwann cells stimulated to proliferate in the absence of neurons retain full functional capability. *J. Neurosci.* **6,** 3070–3078
23. Gollan, L., Salomon, D., Salzer, J. L., and Peles, E. (2003) Caspr regulates the processing of contactin and inhibits its binding to neurofascin. *J. Cell Biol.* **163,** 1213–1218
24. Agrawal, D., Hawk, R., Avila, R. L., Inouye, H., and Kirschner, D. A. (2009) Internodal myelination during development quantitated using X-ray diffraction. *J. Struct. Biol.* **168,** 521–526
25. Aroca-Aguilar, J. D., Sánchez-Sánchez, F., Ghosh, S., Coca-Prados, M., and Escribano, J. (2005) Myocilin mutations causing glaucoma inhibit the intracellular endoproteolytic cleavage of myocilin between amino acids Arg-226 and Ile-227. *J. Biol. Chem.* **280,** 21043–21051
26. Chen, Z. L., and Strickland, S. (2003) Laminin γ1 is critical for Schwann cell differentiation, axon myelination, and regeneration in the peripheral nerve. *J. Cell Biol.* **163,** 889–899
27. Yu, W. M., Feltri, M. L., Wrabetz, L., Strickland, S., and Chen, Z. L. (2005) Schwann cell-specific ablation of laminin γ1 causes apoptosis and prevents proliferation. *J. Neurosci.* **25,** 4463–4472
28. Yang, D., Bierman, J., Tarumi, Y. S., Zhong, Y. P., Rangwala, R., Proctor, T. M., Miyagoe-Suzuki, Y., Takeda, S., Miner, J. H., Sherman, L. S., Gold, B. G., and Patton, B. L. (2005) Coordinate control of axon defasciculation and myelination by laminin-2 and -8. *J. Cell Biol.* **168,** 655–666
29. Joe, M. K., and Tomarev, S. I. (2010) Expression of myocilin mutants sensitizes cells to oxidative stress-induced apoptosis. Implication for glaucoma pathogenesis. *Am. J. Pathol.* **176,** 2880–2890
30. Birchmeier, C. (2009) ErbB receptors and the development of the nervous system. *Exp. Cell Res.* **315,** 611–618
31. Lemke, G. (2006) Neuregulin-1 and myelination. *Sci STKE 2006*, pe11
32. Carroll, S. L., Miller, M. L., Frohnert, P. W., Kim, S. S., and Corbett, J. A. (1997) Expression of neuregulins and their putative receptors, ErbB2 and ErbB3, is induced during Wallerian degeneration. *J. Neurosci.* **17,** 1642–1659
33. Michailov, G. V., Sereda, M. W., Brinkmann, B. G., Fischer, T. M., Haug, B., Birchmeier, C., Role, L., Lai, C., Schwab, M. H., and Nave, K. A. (2004) Axonal neuregulin-1 regulates myelin sheath thickness. *Science* **304,** 700–703
34. Guertin, A. D., Zhang, D. P., Mak, K. S., Alberta, J. A., and Kim, H. A. (2005) Microanatomy of axon/glial signaling during Wallerian degeneration. *J. Neurosci.* **25,** 3478–3487
35. Citri, A., Skaria, K. B., and Yarden, Y. (2003) The deaf and the dumb. The biology of ErbB-2 and ErbB-3. *Exp. Cell Res.* **284,** 54–65
36. Goebbels, S., Oltrogge, J. H., Kemper, R., Heilmann, I., Bormuth, I., Wolfer, S., Wichert, S. P., Möbius, W., Liu, X., Lappe-Siefke, C., Rossner, M. J., Groszer, M., Suter, U., Frahm, J., Boretius, S., and Nave, K. A. (2010) Elevated phosphatidylinositol 3,4,5-trisphosphate in glia triggers cell-autonomous membrane wrapping and myelination. *J. Neurosci.* **30,** 8953–8964
37. Cotter, L., Ozçelik, M., Jacob, C., Pereira, J. A., Locher, V., Baumann, R., Relvas, J. B., Suter, U., and Tricaud, N. (2010) Dlg1-PTEN interaction regulates myelin thickness to prevent damaging peripheral nerve overmyelination. *Science* **328,** 1415–1418
38. Albrecht, D. E., Sherman, D. L., Brophy, P. J., and Froehner, S. C. (2008) The ABCA1 cholesterol transporter associates with one of two distinct dystrophin-based scaffolds in Schwann cells. *Glia* **56,** 611–618
39. Saito, F., Moore, S. A., Barresi, R., Henry, M. D., Messing, A., Ross-Barta, S. E., Cohn, R. D., Williamson, R. A., Sluka, K. A., Sherman, D. L., Brophy, P. J., Schmelzer, J. D., Low, P. A., Wrabetz, L., Feltri, M. L., and Campbell, K. P. (2003) Unique role of dystroglycan in peripheral nerve myelination, nodal structure, and sodium channel stabilization. *Neuron* **38,** 747–758
40. Nakagawa, M., Miyagoe-Suzuki, Y., Ikezoe, K., Miyata, Y., Nonaka, I., Harii, K., and Takeda, S. (2001) Schwann cell myelination occurred without basal lamina formation in laminin alpha2 chain-null mutant (dy3K/dy3K) mice. *Glia* **35,** 101–110
41. McKee, K. K., Yang, D. H., Patel, R., Chen, Z. L., Strickland, S., Takagi, J., Sekiguchi, K., and Yurchenco, P. D. (2012) Schwann cell myelination requires integration of laminin activities. *J. Cell Sci.* **125,** 4609–4619
42. Taveggia, C., Zanazzi, G., Petrylak, A., Yano, H., Rosenbluth, J., Einheber, S., Xu, X., Esper, R. M., Loeb, J. A., Shrager, P., Chao, M. V., Falls, D. L., Role, L., and Salzer, J. L (2005) Neuregulin-1 type III determines the ensheathment fate of axons. *Neuron* **47,** 681–694
43. Tzahar, E., Levkowitz, G., Karunagaran, D., Yi, L., Peles, E., Lavi, S., Chang, D., Liu, N., Yayon, A., and Wen, D. (1994) ErbB-3 and ErbB-4 function as the respective low and high affinity receptors of all Neu differentiation factor/heregulin isoforms. *J. Biol. Chem.* **269,** 25226–25233
44. Sliwkowski, M. X., Schaefer, G., Akita, R. W., Lofgren, J. A., Fitzpatrick, V. D., Nuijens, A., Fendly, B. M., Cerione, R. A., Vandlen, R. L., and Carraway, K. L., 3rd (1994) Coexpression of erbB2 and erbB3 proteins reconstitutes a high affinity receptor for heregulin. *J. Biol. Chem.* **269,** 14661–14665
45. Davies, A. M. (1998) Neuronal survival. Early dependence on Schwann cells. *Curr. Biol.* **8,** R15–R18
46. Meyer, D., and Birchmeier, C. (1995) Multiple essential functions of neuregulin in development. *Nature* **378,** 386–390
47. Riethmacher, D., Sonnenberg-Riethmacher, E., Brinkmann, V., Yamaai, T., Lewin, G. R., and Birchmeier, C. (1997) Severe neuropathies in mice with targeted mutations in the ErbB3 receptor. *Nature* **389,** 725–730
48. Woldeyesus, M. T., Britsch, S., Riethmacher, D., Xu, L., Sonnenberg-Riethmacher, E., Abou-Rebyeh, F., Harvey, R., Caroni, P., and Birchmeier, C. (1999) Peripheral nervous system defects in erbB2 mutants following genetic rescue of heart development. *Genes Dev.* **13,** 2538–2548
49. Lonigro, A., and Devaux, J. J. (2009) Disruption of neurofascin and gliomedin at nodes of Ranvier precedes demyelination in experimental allergic neuritis. *Brain* **132,** 260–273